



Article

Flexural Performance of FRP-Reinforced Geopolymer Concrete Beam

Janeshka Goonewardena, Kazem Ghabraie and Mahbube Subhani *

School of Engineering, Deakin University, 75 Pigdons Road, Waurn Ponds, VIC 3216, Australia;
j.goonewardena@deakin.edu.au (J.G.); k.ghabraie@deakin.edu.au (K.G.)

* Correspondence: mahbube.subhani@deakin.edu.au; Tel.: +61-3-5227-1358

Received: 26 November 2020; Accepted: 14 December 2020; Published: 15 December 2020



Abstract: Fibre-reinforced polymer (FRP) rebar and geopolymer concrete (GPC) are relatively new construction materials that are now being increasingly used in the construction sectors. Both materials exhibit superior structural and durability properties that also make them a sustainable alternative solution. Due to the absence of any design standard for an FRP-reinforced GPC beam, it is important to validate the efficacy of available standards and literature related to other materials, e.g., FRP-reinforced conventional concrete or GPC alone. Four theories/design standards are considered for this comparison—ACI440.1R-15, CAN/CSA S806-12, parabolic stress block theory, and equivalent rectangular stress block theory for GPC under compression. The accuracy of these four approaches is also examined by studying the flexural performance of both the glass FRP (GFRP) and carbon FRP (CFRP). The FRP-reinforced beams are designed against the actual load they will be subjected to in a real-world scenario. It is concluded that parabolic stress block theory over-estimates the capacity, whereas CSA S806-12 yields the most accurate and conservative results. In addition, the flexural performance of the FRP-reinforced beams is evaluated in terms of ultimate, cracking, and service moment capacity, along with serviceable, ultimate, and residual deflection.

Keywords: geopolymer concrete; CFRP; GFRP; flexural capacity; theoretical prediction

1. Introduction

The durability aspect of geopolymer concrete (GPC) is well established which includes, but is not limited to, low creep, superior resistance against sulphate and acid attack, reduced drying shrinkage, less water absorption, and higher fire resistance and dimensional stability [1–5]. In terms of the tensile reinforcement of concrete, steel is the most commonly used material. The corrosion issue in steel can be eliminated by using fibre-reinforced polymers (FRP) such as carbon-FRP (CFRP), glass-FRP (GFRP), aramid-FRP (AFRP), and basalt-FRP (BFRP) as longitudinal and transverse reinforcements [6]. Major applications of FRP rebar in concrete include marine structures and bridges exposed to de-icing salts [7] or any other corrosion-prone areas. FRP bars have a higher strength to weight ratio, are electrochemically neutral, and have excellent fatigue and chemical resistance [8,9]. In terms of sustainability, GPC is a viable alternative for concrete that uses alkali-activated by-product materials such as rice husk ash and fly ash [10]. In addition to the conventionally used aluminosilicate precursors, phosphates were introduced to the activation process; this type of geopolymer concrete is termed as phosphate-based geopolymer concrete or aluminosilicate phosphate cement. While the conventional aluminosilicate geopolymer concrete is ideal for large-scaled constructions, the application of phosphate-based geopolymer is considered feasible in biomaterials [11]. GPC emits 64% less carbon dioxide in its production life cycle compared to its Ordinary Portland Cement (OPC) counterpart [12]. Furthermore, it has the potential to reduce cost by up to 30% depending on the use of alkaline liquids [13].

In terms of the structural properties of GPC, contradictory conclusions were reported in the literature. These differences in results can be attributed to the broad range of mix designs adopted by different researchers in terms of curing condition, slag to fly-ash ratio, and alkali-activated constituents [14]. GPC is reported to have lower elastic modulus [5,15] and exhibit more brittle failure behaviour [16–18] compared to Ordinary Portland Cement (OPC)-based concrete. While some studies [19–23] reported similar behaviour for GPC beams when compared with OPC beams, others [15,24,25] reported significant differences. Apart from the mechanical properties of GPC itself, the bond strength at the FRP to GPC interface plays an important role for effectively carrying the applied load on an FRP-reinforced GPC structural element. It is reported that the glass FRP (GFRP) bar to GPC interface [26] and aramid FRP or carbon FRP rebar to OPC interface [27] have similar bond strengths compared to the similar size steel-to-concrete interface. Nevertheless, due to the lower elastic modulus of GFRP, the serviceability requirement in terms of deflection or flexural stiffness was reported to be lower [20]. In this regard, the implementation of carbon FRP (CFRP) rebar has the potential of improving flexural stiffness, since CFRP has a similar modulus of elasticity to that of steel and has better bond strength with concrete compared to the FRP rebar. For FRP-reinforced GPC beams, most of the studies focused on geopolymer and conventional concrete beams reinforced with GFRP [28–33], while only a few reported on GPC beams reinforced with CFRP [34,35]. In the present study, both GFRP and CFRP rebars have been considered for the design of beams.

Since FRP bars behave linearly elastic until failure, most of the design guidelines recommend the design of FRP-reinforced geopolymer beams to be over-reinforced. Accordingly, the failure strain of GPC under compression becomes the governing design factor. The failure strain of geopolymer concrete varies significantly and is reported to be in the range of 0.0015–0.0050. Sarkar [4] recommended a failure strain value of 0.003, Tran et al. [36] proposed 0.0035, Ahmed et al. [37] reported a range of 0.002–0.0033, and Maranan et al. [20] found the failure strain to be in the range of 0.0029–0.0048. Due to a variation in mix design and curing condition, the compressive strength and strain of GPC also varies, and hence, more research is required to investigate the failure strain of geopolymer concrete considering its mix design.

The present study compares the flexural behaviour of both CFRP and GFRP-reinforced geopolymer beams in terms of ultimate, cracking, and service moment capacity, along with serviceable, ultimate, and residual deflection. In addition, strain distribution and failure behaviour are also reported. For this purpose, GFRP and CFRP-reinforced GPC beams were designed, casted, and tested along with normal steel-reinforced OPC concrete beams. Details of the experimental program are reported in Section 2. Test results are analysed in Section 3.

The aforementioned strain of concrete plays a vital role in the flexural performance of a reinforced beam. Therefore, it is vital to investigate the varying types of strain and how they affect the contemporary design standards for geopolymer concrete structures. This study will compare experimental moment capacities against two of the most commonly used design standards—ACI440.1R-15 [38] and CAN/CSA S809-12 [39]. However, since these two standards are developed for FRP-reinforced OPC concrete structures, an additional two theoretical models are also taken into account, which consider a parabolic stress block [34] and equivalent rectangular stress block [36] for geopolymer concrete under compression. Alongside this, a detailed flexural performance that is inclusive of ultimate and service states has been carried out for all beams.

This article is based on a project that was undertaken in collaboration with industry partner Austeng (Australian Engineering Solutions Pty. Ltd., North Geelong, VIC, Australia)—a local consultation company in Geelong, Australia. The City of Greater Geelong (CoGG) has taken numerous innovative and sustainable initiatives in the construction sector. As a part of the “100 years maintenance-free pedestrian bridge” project, CoGG decided to construct or replace 160 pedestrian bridges around the City of Greater Geelong with minimal maintenance requirements using sustainable and durable materials. Accordingly, geopolymer concrete and fibre-reinforced polymer rebars were selected as the materials for the design of these bridges.

The beams of the pedestrian bridges were designed in accordance with AS5100.2:2017 (Bridge design—Design loads). Alongside AS5100, AS1170.0:2002 (Structural design actions—General principles) and AS1170.1:2002 (Structural design actions—Permanent, imposed and other actions) were used to accurately design the beams by considering the loads that the bridges would be subjected to during their design life at the designated site. Both CFRP and GFRP rebar were considered to design the bridge. However, the aim of this project was to select the most accurate design equations while designing FRP-reinforced geopolymer beams.

2. Experimental Program

The experimental program consists of three groups—conventional steel reinforced ordinary concrete, CFRP-reinforced geopolymer concrete, and GFRP-reinforced geopolymer concrete beams. Two samples were tested from each group.

2.1. Materials

2.1.1. Concrete

A commercial ready-mix geopolymer concrete (GPC) mixture, supplied by Rocla in Australia, was used for this experimental study. Its constituents are a mixture of fine and coarse aggregates, fly ash, slag, sodium hydroxide pellets (NaOH), and sodium silicate solution (Na_2SiO_3). Rocla did not disclose the exact proportions of constituents and processes used due to commercial sensitivity. The GPC mixture was made in two batches, and the average cylinder compressive strengths at different stages are given in Table 1.

Table 1. Compressive strength of concrete.

Mix	4-Hour Strength (MPa)	24-Hour Strength (MPa)	15-Day Strength (MPa)	28-Day Strength (MPa)	f_r —Modulus of Rupture (MPa)
GPC Mix 1	44.8	59.4	61.3	62.0	4.72
GPC Mix 2	43.4	56.6	58.7	60.0	4.65
OPC Mix	-	-	-	69.0	4.98

Determination of the rupture modulus (f_r) is discussed in Section 3.4 (Equation (2b)).

2.1.2. Reinforcing Bars

The GFRP and CFRP bars were provided by V-Rod in Australia with a diameter of 25.4 (#8) and 15.9 (#5) mm, respectively. The binding material for the rebar is composed of modified vinyl ester resin with a maximum volume fraction of 35%. The GFRP bars were reinforced with continuous E-glass fibres with a minimum volume fraction of 65%. Both bars were made using the pultrusion technique. The bars were coated with sand to attain sufficient bond strength.

The Modulus of Elasticity (MoE) of FRP is one of the limiting factors in structural design, as it is lower than the MoE of 200 GPa for steel. Accordingly, the serviceability limit on deflection governs the design in numerous occasions when FRP bars are used. Since the deflection of bars is dependent on the stiffness, it is important to choose FRP bars with a high MoE or a high cross-sectional area. The mechanical properties of the GFRP and CFRP bars are listed in Table 2, based on the manufacturer data sheet. As shown in the table, CFRP has a higher modulus, whereas a GFRP modulus is around one-third of the steel rebar. Hence, a bar with a large diameter for GFRP and a small diameter for CFRP were chosen.

Table 2. Mechanical properties of the tensile rebar.

Bar	Guaranteed f_{fu} (MPa)	d_b (mm)	E (GPa)	ϵ_{fu} (%)	Nominal A_f (mm ²)	EA_f (MN)	Nominal τ_b (MPa)
GFRP #8	1000	25.4	66.4 ± 2.5	1.51	506.7	33.6	14.0
CFRP #5	1532	15.9	140 ± 2.5	1.18	197.9	27.7	16.3
Steel	500	16	200	25.0	201.0	40.2	-

f_{fu} = guaranteed ultimate tensile strength, d_b = bar diameter, E = modulus of elasticity, ϵ_{fu} = ultimate elongation, A_f = cross-sectional area of the bar, τ_b = bond strength with conventional Ordinary Portland Cement (OPC) concrete.

2.2. Beam Specification

As mentioned earlier, both the CFRP and GFRP-reinforced geopolymer beams were designed to carry the load, which will be acting on the beam during its design life. Accordingly, it can be noticed below that the bar diameter and number of bars for CFRP and GFRP were selected to withstand the design action. The main goal was not to carry out the comparison between CFRP and GFRP, rather to check the accuracy of the design equations that predict the flexural capacity of a GFRP or CFRP-reinforced geopolymer concrete beam, since no design standards are available.

The experimental program consists of two beams each in three groups. The control group (BS) was made from normal OPC concrete using steel rebars, while the BCF and BGF series were CFRP and GFRP-reinforced GPC, respectively. The geometric details of the beams are given in Table 3.

Table 3. Geometrical properties of beams.

Beam	Section		Tension Reinforcement			Concrete Mix
	b (mm)	h (mm)	Bars	ρ_f	ρ_{fb} *	
BS1	200	250	2@16.0mm	0.010	0.037	OPC Mix
BS2	200	250	2@16.0mm	0.010	0.037	OPC Mix
BGF1	200	250	2@25.4mm	0.025	0.006	GPC Mix 2
BGF2	200	250	2@25.4mm	0.025	0.006	GPC Mix 1
BCF1	200	250	2@15.9mm	0.011	0.005	GPC Mix 1
BCF2	200	250	2@15.9mm	0.012	0.005	GPC Mix 2

* based on CSA S806-12 [39], ρ_f = reinforcement ratio of the beam and ρ_{fb} = balanced reinforcement ratio.

CSA S806-12 [39] was chosen for the calculation of the balanced reinforcement ratio due to the standard’s wide usage for the design of a geopolymer concrete structure with respect to the other existing standards. Furthermore, design manuals prepared by ISIS Canada [40] (based on standards such as CSA 806 and CSA S6) discuss design examples for FRP-reinforced concrete structures.

All beams were 250 mm high, 200 mm wide, and 3000 mm long, and they were longitudinally reinforced with two bars each on the top (compression) and bottom (tension) (Figures 1 and 2). For shear reinforcement, 12 mm (#4) GFRP and CFRP V-Rod Bent bars were used for the BGF and BCF beam groups, respectively. The OPC beams were shear reinforced with 16 mm (#5) 180 mm × 130 mm steel rectangular ligatures (Figure 3). The properties of shear reinforcement are tabulated in Table 4, which have been extracted from the manufacturer’s (V-Rod) technical data sheet. The BCF and BGF beams were designed to be over-reinforced ($\rho_f > \rho_{fb}$), following the recommendations in ACI 440.1R-15 [38], which would result in the compression failure of GPC. This is due to the brittle failure exhibited by FRP rebar under tension (linearly elastic until failure).

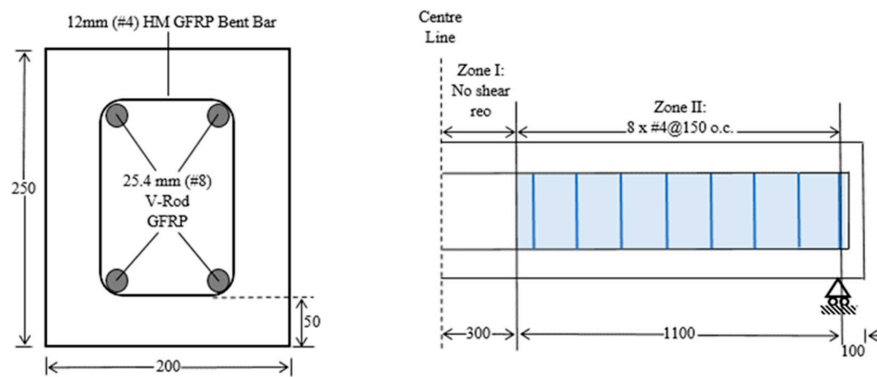


Figure 1. Reinforcement details of BGF1 and BGF2 (all the dimensions are in mm).

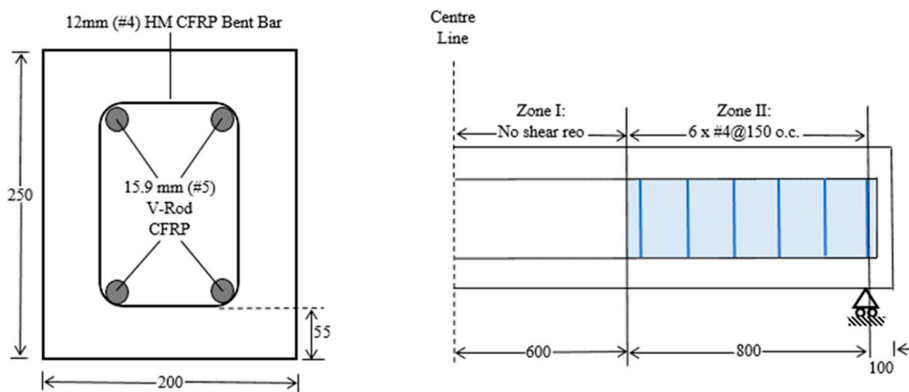


Figure 2. Reinforcement details of BCF1 and BCF2 (all the dimensions are in mm).

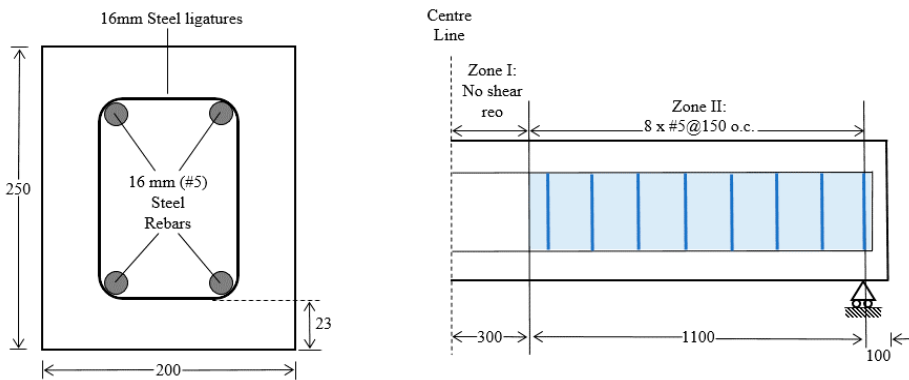


Figure 3. Reinforcement details of BS1 and BS2 (all the dimensions are in mm).

Table 4. Mechanical properties of shear reinforcement.

Stirrup	Cross-Sectional Area (mm ²)	Nominal Tensile Modulus (GPa)	Tensile Strength (MPa) (Bent Portion)
GFRP #4	126.68	50	459
CFRP #4	126.68	120	428
Steel #5	197.93	80	-

A clear cover of 50 mm and 55 mm was used for the BGF and BCF series, respectively. It should be noted here that due to the floating of CFRP bars (manufacture error) during the casting of BCF2, this beam had a clear cover of 70 mm. The offset was measured at the mid-point and was taken into consideration in the theoretical mid-span bending moment. The BS beams have a clear cover of 23 mm. In order to have a similar effective depth (≈ 175 mm) for all the FRP beams, varying clear

covers were chosen; GFRP beams consisted of a lesser clear cover in order to compensate for the bigger diameter with respect to CFRP bars.

2.3. Test Setup

A four-point static bending test was conducted on test beams. The beams were loaded by two concentrated loads with a distance of 400 mm from the mid-span, as shown in Figure 4. This yielded a shear span of 1000 mm on both sides. The load was applied in two steps:

- I. Load control: 5 kN/min up to 70 kN
- II. Displacement rate: After the 70 kN mark was reached, the loading changed to displacement control at a rate of 2 mm/min.

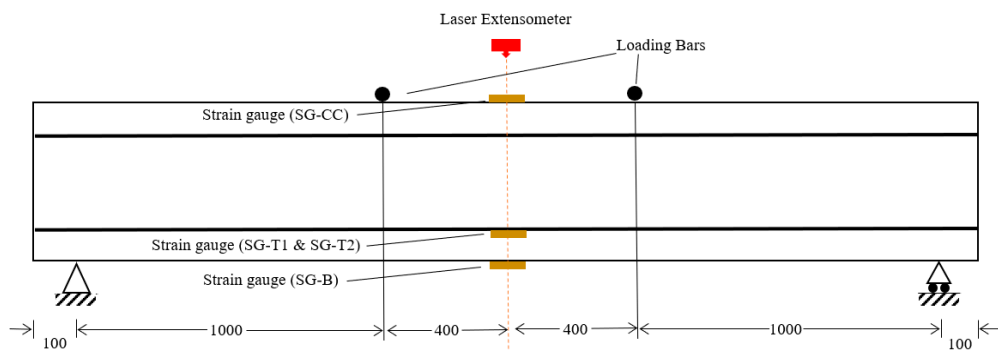


Figure 4. Schematic diagram of the test setup.

The mid-span deflection was measured using a laser extensometer that was attached to the loading plate. The Data Acquisition System takes into account the displacement of the moving loading plate, which has been added to the relative deflection that the laser detects to produce a total deflection. Strains were measured at four locations across the cross-section (Figure 4). a total of four strain gauges were used in each beam except for the BS series, and they were placed on top (SG-CC) and bottom (SG-B) of the GPC beams and on the two bottom longitudinal FRP rebar (SG-T1 and SG-T2). Figure 5 depicts the experimental setup of the beams.



Figure 5. Test setup—loading span, laser extensometer, and strain gauge.

3. Experimental Results and Discussion

This section aims to summarise the failure modes observed, load–deflection relationship, flexural capacity, and the strain distribution in the GPC beams following the loading tests.

3.1. Mode of Failure

In general, vertical cracks formed at the constant moment zone after the tensile strength of the concrete was exceeded (Figure 6a). These cracks widened with the increase in load and

propagated upwards, while new cracks formed at the shear zone (shear cracks in Figure 6b). The shear cracks were much more significant in the BCF beams. The BCF beams exhibited failure characterized by the crushing of unconfined (at the boundary between zone I and zone II—Figure 2) geopolymer concrete, which was followed by shear failure (Figure 6b). In BCF1, concrete crushing was observed closer to the shear zone. As mentioned in Section 2.2, the tensile rebar had a larger clear cover of 70 mm in BCF2, resulting in a lower load-carrying capacity. Due to the reduced lever arm of the tensile rebar to carry the resulted tensile force from bending, the compression CFRP bars at the shear zone were ruptured (Figure 6d). The BGF beams exhibited failure characterised by the crushing of unconfined (at the boundary between zone I and zone II—Figure 2) geopolymer concrete as well, but in these beams, failure was initiated by tensile cracks at the constant moment zone (Figure 6c). The ultimate failure of the BS series was also concrete crushing. However, as the BS series were designed as under-reinforced, as opposed to FRP-reinforced GPC beams, steel-yielding took place before the ultimate failure. This is obvious, as the ultimate failure strain of steel is higher than concrete and leads to concrete crushing before the rupture of the steel rebar.

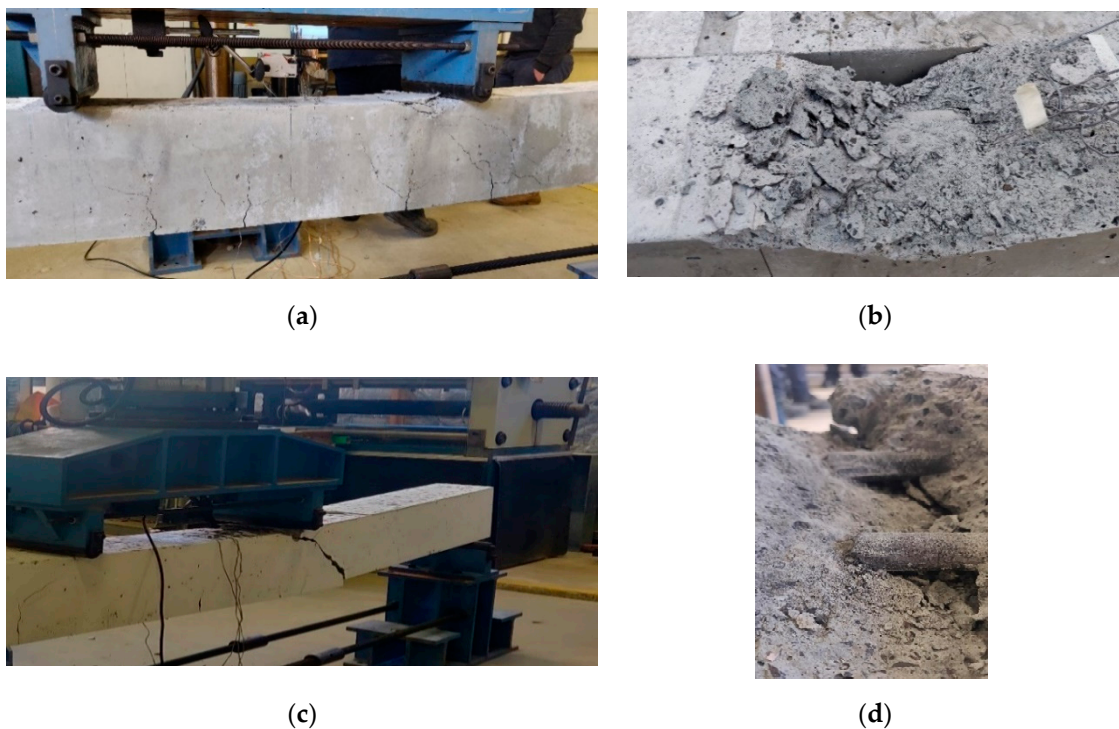
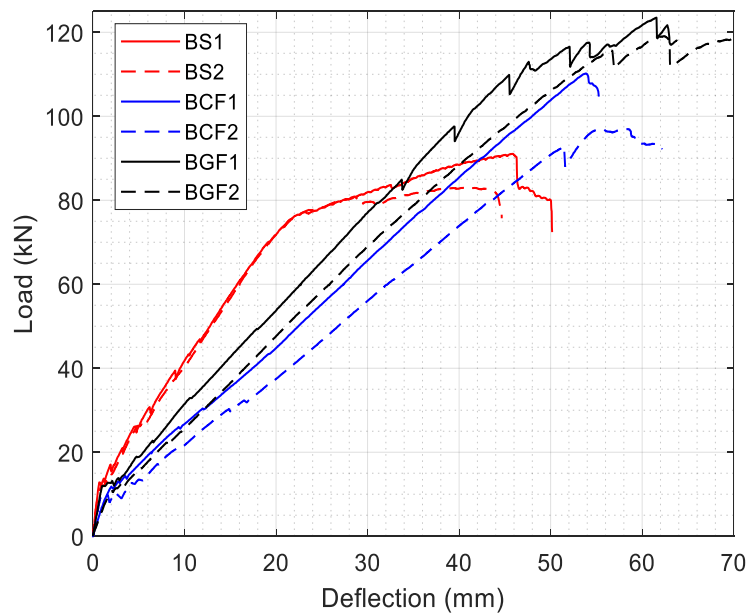


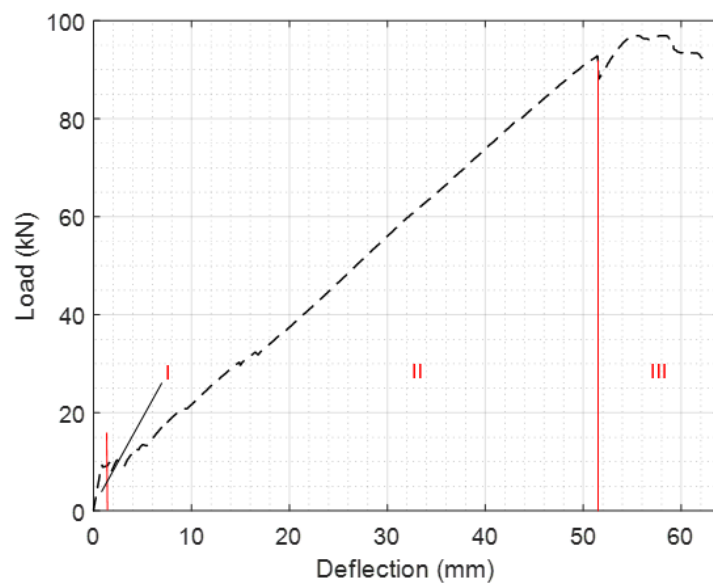
Figure 6. (a) Cracks at the constant moment zone; (b) Shear crack; (c) Concrete crushing; (d) Rupture of compression bars.

3.2. Load–Deflection Response

Figure 7a presents load vs. mid-span deflection graphs of all six beams. The load–deflection curves can essentially be divided into three segments (Figure 7b). The first segment is a steep linear response for all beams, which represents the uncracked state of the beams. For the GPC beams, when the applied load exceeded the tensile strength of the concrete or the modulus of rupture, cracks began to form within the constant moment zone. Thereafter, the curves transitioned to the second segment, which represents the cracked state of the beams. This segment, which lasts until the peak compressive strain, has a reduced slope with respect to the first segment due to increased cracking. Each time a major crack appeared, there was a drop in load.



(a)



(b)

Figure 7. (a) Load–deflection curves for the tested beams. (b) Example of three segments of load–deflection curves using BCF2.

The third segment follows immediately from the second, in which beam failure occurred by concrete crushing. This has a non-linear response and depends on the material and mechanical properties of the GPC and the FRP bars. The BS series yielded a similar three-segment curve, with a different post-cracking response. As evident, the second segment of the BS beams have a steeper slope than the FRP-reinforced GPC beams, as the modulus of elasticity of steel is higher than that of GFRP and CFRP bars. The third segment signifies yielding of the steel, due to the reduction of the slope. However, due to the favourable ductile nature of steel, the third segment lasted over a deflection of approximately 20 mm for both BS1 and BS2. Furthermore, even though the stiffness was compromised

with respect to segment two, the tensile stress of the BS beams kept increasing until concrete crushing took place.

Usually after failure, the stirrups provide a confinement effect where the beams show additional ductility and strength. This is evident in the BGF series but not in BS and BCF. This may have been caused by the shear capacity being exceeded in the middle region of the beam where no shear reinforcement is used, causing sudden failure. It is noteworthy that the BGF1-produced progressive load drops, while BGF2 has no drops until immediately before rupture. This may be attributed to a slip that may have taken place at the GFRP rebar to the GPC interface. It is well reported in the literature that the bond strength of the FRP rebar to concrete, or GPC in this regard, can vary. This due to the fact that the sand coating on the FRP rebar surface is not controlled to a great accuracy, resulting in a variation of bond strength value along the length of the rebar and from one beam sample to another.

3.3. Stiffness

The stiffness was calculated by measuring the gradient of segment 2 (see Figure 7b) as the load–deflection response is linear–elastic in this region. The results are listed in Table 5. Due to the lower MoE values of GFRP and CFRP, the lower stiffness in FRP-reinforced GPC beams was expected.

Table 5. Stiffness of tested beams.

Beam ID	Stiffness (kN/mm)	Average Stiffness (kN/mm)	Ratio w. r. to BS	Axial Rigidity, EA (MN)	EA Ratio w. r. to Steel
BS1	3.21	3.25	1.0	40.2	1.0
BS2	3.29				
BGF1	2.33	2.28	0.7	33.6	0.84
BGF2	2.22				
BCF1	2.06	1.94	0.6	27.7	0.69
BCF2	1.81				

As shown in Table 5, there was a decrease of 30 and 40% in stiffness of BGF and BCF beams, respectively. The axial rigidity of the steel, GFRP bars, and CFRP bars are also shown in Table 5. Even though the axial rigidity is reduced by only 16 and 31% for the GFRP and CFRP bars, respectively, the stiffness reduction is found to be more in corresponding beams. This further reduction is possibly due to the use of GPC. This is due to the fact that the axial rigidity ratio of GFRP to CFRP ($33.6/27.7 = 1.21$) closely matches the stiffness ratio of the corresponding beam series ($2.28/1.94 = 1.18$).

3.4. Moment Capacity

Table 6 tabulates the cracking moment (M_{cr}), moment at serviceability limit (M_s), and ultimate moment capacity (M_u). The failure modes of the beams are also included. It should be noted that the failure of all beams was initiated by flexural cracks at the mid-span. The ultimate moment from the experiment was determined as follows

$$M_u = \frac{P}{2}a \tag{1}$$

where P is the ultimate load (kN) and a is the shear span (m), which is 1 m.

Table 6. Bending moment at cracking, service, and ultimate states.

Specimen	M_{cr} (kNm)	M_s (kNm)		P_u (kN)	M_u (kNm)	Failure Mode
		2000 $\mu\epsilon$	0.3 M_u			
BS1	11.02	-	13.66	91.06	45.53	SY
BS2	11.02	-	12.44	82.96	41.48	SY
BGF1	9.89	22.32	18.53	123.50	61.75	CC
BGF2	10.05	19.17	17.94	119.59	59.80	CC
BCF1	10.12	16.16	16.53	110.20	55.10	CC
BCF2	9.86	8.82	14.54	96.95	48.48	S

SY = failure due to steel yielding, S = Shear failure, CC = Concrete crushing.

3.4.1. Cracking Moment

The cracking moment in Table 6 was determined using CSA S806-12 [39]. M_{cr} depends mainly on the modulus of rupture of GPC (f_r), which is similar in both mixes (see Table 1), as they have a similar concrete strength (f'_c).

$$M_{cr} = \frac{f_r I_t}{y_t} \quad (2a)$$

$$f_r = 0.6\lambda \sqrt{f'_c} \quad (2b)$$

where I_t is the second moment of area of the transformed section, y_t is the depth of the neutral axis from the furthest tensile fibres, λ is the modification factor for density of concrete (1.0 for normal density concrete), and f'_c is the compressive strength of concrete.

When the applied moment reached the cracking moment capacity, cracks formed on the tension side of the beams and propagated towards the top surface. The cracked concrete can no longer carry tensile stress; this causes a decrease in the flexural rigidity, as evident from the slope reduction in Figure 7b.

3.4.2. Service State

The flexural strength at the service stage (M_s) is a good indication of the performance of any FRP-reinforced concrete/GPC beam. Two criteria have been used to determine the service bending moment. The first criterion is taken from ISIS-07 [40], which defines the service moment as the applied moment that corresponds to a tensile strain of 2000 $\mu\epsilon$. Both BGF beams have similar M_s capacity with an average of 20.75 kNm. However, BCF2 has an erratic value when compared to BCF1 due to the manufacturing error mentioned previously. Taking BGF1, BGF2, and BCF1 into consideration, the BGF series has a 25% higher M_s capacity ($20.75/16.53 = 1.25$) at the same tensile strain than BCF1 despite CFRP having a larger modulus of elasticity than GFRP. This is due to the GFRP bars used in this study having a 21% larger axial rigidity than CFRP. The second criterion is from Bischoff's [41] study where the service moment is estimated to be 30% of the ultimate moment (M_{ult}). These estimations are comparable with each other and within 15% of the values determined from ISIS-07 (except for BCF2).

3.4.3. Ultimate Moment

BS1 and BS2 attained M_{ult} values of 45.53 and 41.48 kNm, respectively. The flexural response was very similar for both beams; BS2 had a slightly lower M_{ult} due to a higher number of cracks. BCF1 produced an M_{ult} of 55.10 kNm and BCF2 responded with 48.48 kNm, which is a 12% decrease due to the aforementioned manufacturing error. However, BGF1 and BGF2 yielded comparable ultimate flexural strengths at 61.75 and 59.80 kNm, respectively. It can also be noticed here that even though the BGF beams had a reinforced ratio 2.5 times higher than the BCF beams, their ultimate moment capacity is only 1.17 times higher than the BCF beams.

3.5. Mid-Span Deflection

Figure 8 depicts moment vs. mid-span deflections. Since the beams were made of different concrete mixes, the bending moment has been normalised by the factor $bd^2 f'_c$, where b is the width of the beam, d is the effective depth of the beam, and f'_c is the compressive strength of the concrete mix. For the same deflection, BS1 and BS2 have a higher flexural capacity (until the yield strength) than the beams with the FRP bars. This is due to the higher modulus of elasticity of steel (200 GPa) with respect to GFRP (66.4 GPa) and CFRP (140 GPa) bars.

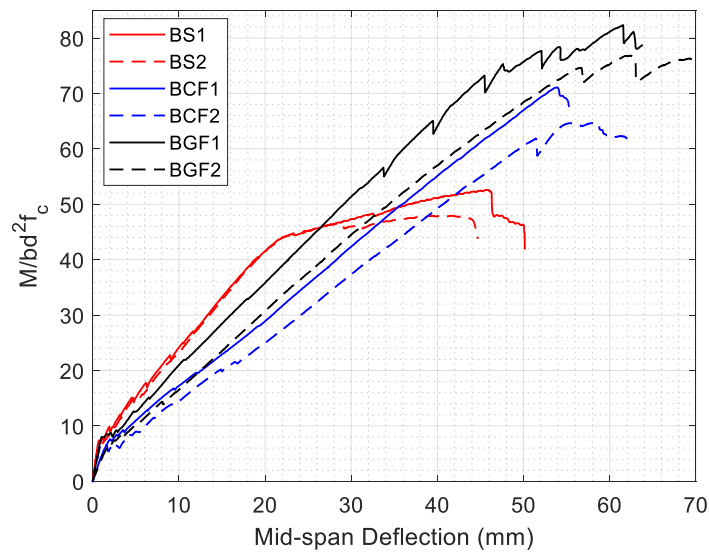


Figure 8. Normalised moment vs. deflection.

Table 7 shows the theoretical and experimental mid-span deflection of the beams at service state ($\Delta_{s\text{-tho}}$ and $\Delta_{s\text{-exp}}$) and ultimate state (Δ_{theo} and Δ_{exp}). All the theoretical deflection equations were calculated using Equation (3) by substituting the corresponding load (P) at the service and ultimate states.

$$\Delta = \frac{\left(\frac{Pa}{2}\right)(3L^2 - 4a^2)}{24E_cI_e} \tag{3}$$

where Δ = mid-span deflection, P = applied load on the four-point bending test, L = span length, a = shear span (distance from the support to the loading point), E_c = elastic modulus of concrete, and I_e = effective moment of inertia. Δ_{residual} is the experimental permanent deflection of the beam after the load was removed.

Table 7. Theoretical and experimental mid-span deflection.

Beam ID	$\Delta_{s\text{-exp}}$ (mm)		$\Delta_{s\text{-theo}}$ (mm)		$\Delta_{u\text{-exp}}$ (mm)	$\Delta_{u\text{-theo}}$ (mm)	Δ_{residual} (mm)
	2000 $\mu\epsilon$	0.30 $M_{u\text{-exp}}$	2000 $\mu\epsilon$	0.30 $M_{u\text{-theo}}$			
BS1	-	5.26	-	2.62	45.86	-	-
BS2	-	4.49	-	2.10	40.49	-	-
BGF1	15.84	12.62	12.26	10.78	61.57	36.63	9.52
BGF2	15.85	14.74	10.17	9.34	62.35	35.44	15.46
BCF1	13.28	13.67	9.45	9.74	53.87	38.17	41.17
BCF2	7.33	14.10	3.24	9.83	55.45	40.70	59.00

The aforementioned criteria (ISIS-07 and Bischoff’s recommendation) for the service state have been used to analyse the deflection of the tested beams. As evident, all service state experimental deflections are comparable with each other (with the exception of BCF2 due to the previously mentioned casting issue). However, at the ultimate moment, BGF deflected ($\Delta_{u\text{-exp}}$) 10% more than BCF due to its higher moment capacity and higher axial rigidity. BGF beams and BCF beams had very different Δ_{residual} values. The BGF series had very low residual deflections, as the FRP bars did not rupture. However, the compression bars in the shear zone of the BCF series ruptured, causing the beams to lose their elasticity and consequently attain high residual deflections. The theoretical and experimental ultimate deflections are not comparable with each other. This has been also reported in previous studies that have employed standards such as ACI 440.1R-15 [38].

3.6. Strain Distribution

Figure 9 shows the applied load vs. strains at the top of the geopolymer concrete (SG-CC) and at the two tensile FRP bars (SG-T1 and SG-T2). The initial segment of the curves for both concrete and FRP bars show similar steep slopes. The average ultimate concrete strains obtained from the BGF series and BCF series were 0.0041 (average of 0.0033 and 0.0048) and 0.0036 (average of 0.0032 and 0.0040), respectively. These values are higher than 0.0030 or 0.0035 which are normally adapted for the design of GPC or OPC. The range of failure strain of GPC is rather large (0.0032–0.0048). Considering the strain acting at the FRP bar at failure, the GFRP bars utilised only 47% (on average) of their guaranteed flexural strain, while the CFRP bars used 69%. From Figure 10, the strain behaviour of both the GFRP and CFRP are comparable, since the beams were designed for concrete crushing (over-reinforced). BCF1 and BGF2 have been used for this comparison.

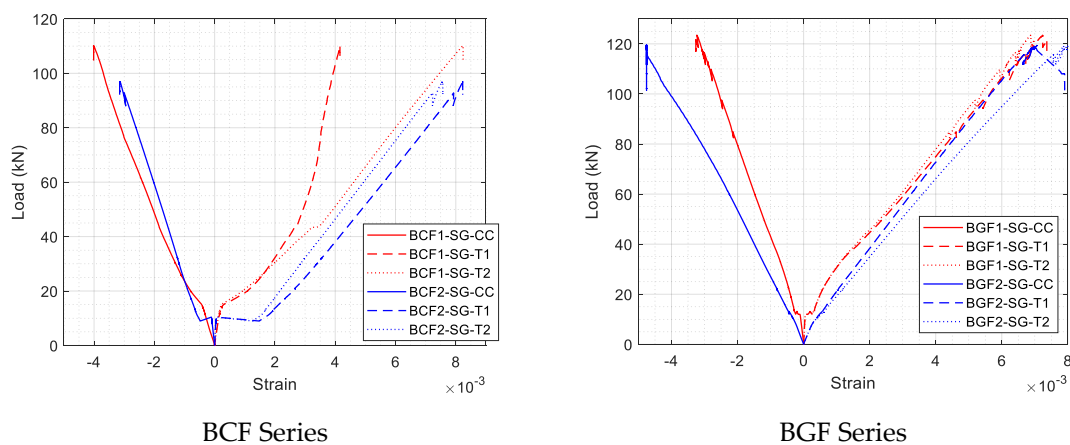


Figure 9. Load vs. strain curve of the fibre-reinforced polymer (FRP)-reinforced geopolymer beams.

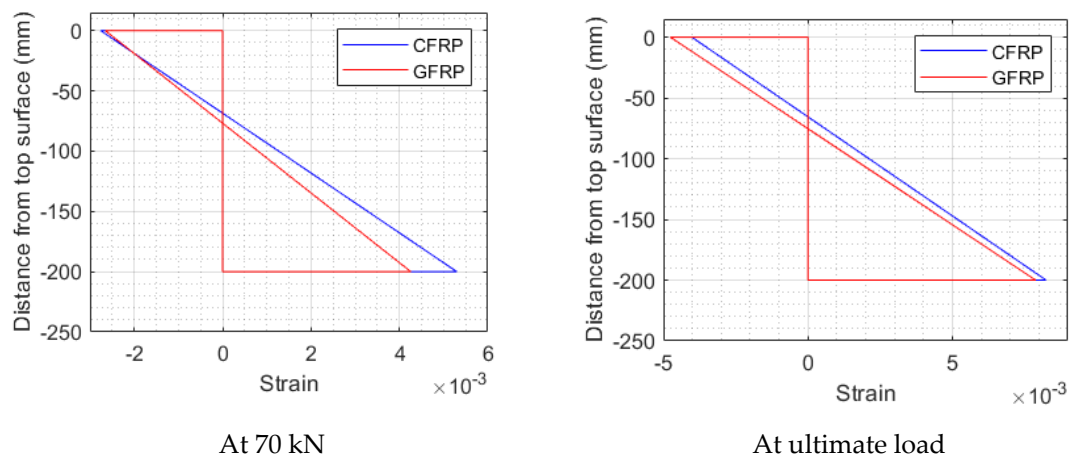


Figure 10. Strain profile (of BCF1 and BGF2) along the cross-section at 70 kN and at ultimate load.

4. Analytical Investigation

In this section, the experimental moment values are compared against four theories. The first two are from ACI440.1R-15 and CSA S806-12, which are based on FRP-reinforced OPC concrete. The third and the fourth theories are based on FRP-reinforced GPC.

4.1. ACI 440.1R-15

The flexural strength is dependent on the failure mechanisms—concrete crushing or FRP rupture. It can be determined by comparing the reinforcement ratio with the balanced reinforcement ratio.

$$\beta_1 = 0.85 - 0.05 \frac{f'_c - 28}{7} \geq 0.65 \quad (4a)$$

$$\rho_{fb} = 0.85\beta_1 \frac{f'_c}{f_{fu}} \frac{E_f \varepsilon_{cu}}{\varepsilon_{cu} + f_{fu}} \quad (4b)$$

where f'_c = compressive strength of concrete, ε_{cu} = ultimate compressive strain of concrete, E_f = modulus of elasticity of FRP rebar, f_{fu} = ultimate tensile strength of FRP, and β_1 is the rectangular stress block parameter related to concrete in compression. Another rectangular stress block parameter, α_1 , is considered constant at 0.85 in ACI440.1R.

For FRP-reinforced concrete, an over-reinforced design is recommended. For an over-reinforced beam ($\rho_f > \rho_{fb}$), tensile stress at the FRP bar (f_f) can be determined as follows

$$f_f = \sqrt{\frac{(E_f \varepsilon_{cu})^2}{4} + \frac{0.85\beta_1 f'_c}{\rho_f} E_f \varepsilon_{cu} - 0.5 E_f \varepsilon_{cu}} \leq f_{fu}. \quad (5)$$

Finally, the ultimate moment capacity ($M_{u,ACI}$) can be calculated using Equation (6):

$$M_{u,ACI} = \rho_f f_f b d^2 \left(1 - 0.59 \frac{\rho_f f_f}{f'_c} \right). \quad (6)$$

4.2. CSA S806-12

The controlling limit state in this standard is compressive failure at the top concrete surface. Therefore, it is only viable for over-reinforced beams. The ρ_{fb} in the CSA code is similar to that of ACI code; however, α_1 can be determined using Equation (7a).

$$\alpha_1 = 0.85 - 0.0015 f'_c \geq 0.67 \quad (7a)$$

$$\beta_1 = 0.97 - 0.0025 f'_c \geq 0.67 \quad (7b)$$

$$\rho_{fb} = \alpha_1 \beta_1 \frac{f'_c}{f_{fu}} \frac{E_f \varepsilon_{cu}}{E_f \varepsilon_{cu} + f_{fu}} \quad (7c)$$

The distance to the neutral axis (c) from the top compression surface can be calculated by equating the compressive and tensile forces acting at the cross-section (Equation (8a)). Stress at the FRP rebar at the failure of the beam and ultimate moment capacity of the beam can be determined using Equations (8b) and (9).

$$\alpha_1 \beta_1 f'_c b c - A_f E_f \frac{\varepsilon_{cu}(d-c)}{c} = 0 \quad (8a)$$

$$f_f = E_f \frac{\varepsilon_{cu}(d-c)}{c} < f_{fu} \quad (8b)$$

$$M_{u,CSA} = \rho_f f_f b d^2 \left(1 - \frac{\rho_f f_f}{2\alpha_1 f'_c} \right) \quad (9)$$

where d = distance between the extreme compression fibre and centroid of the FRP rebar.

4.3. Parabolic Stress Block Theory

FRPs have a linear stress–strain curve up to rupture, while concrete shows a non-linear behavior under compression. The Parabolic Stress Block Theory accommodates the non-linear (parabolic) behavior of concrete compression into its design equations. This theory also considers balance, tension, and compression failure. However, only compression failure will be discussed here, since all the beams were designed to be over-reinforced. The stress–strain distribution of the parabolic stress block is depicted in Figure 11.

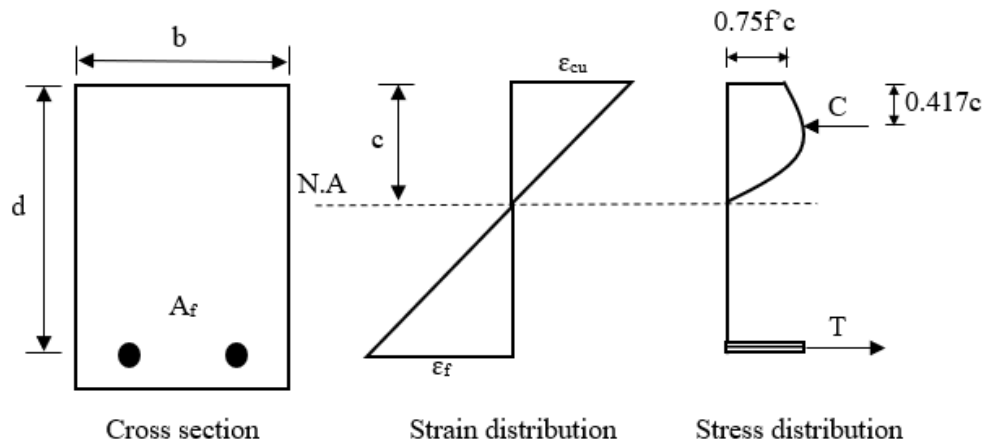


Figure 11. Stress–strain distribution in parabolic stress block based on [34].

The balanced reinforcement ratio in this method is calculated as follows:

$$\rho_{fb} = \frac{0.75c_b f'_c}{d f_{fu}} \tag{10a}$$

$$c_b = \frac{\epsilon_{cu} d}{\epsilon_{cu} + \epsilon_{fu}} \tag{10b}$$

where c_b = distance from the neutral axis to the extreme compressive fibres at balanced failure, and ϵ_{fu} = ultimate strain at FRP rebar.

The tensile stress in FRP rebar at the point of failure, depth of the neutral axis from the extreme compression fibre, and the ultimate flexural strength are calculated using the following equations:

$$f_f = \frac{-\rho_f d E_f \epsilon_{cu} + \sqrt{(\rho_f d E_f \epsilon_{cu})^2 + 3\rho_f d^2 f'_c E_f \epsilon_{cu}}}{2\rho_f d} \leq f_{fu} \tag{11a}$$

$$c = \frac{E_f \epsilon_{cu} d}{E_f \epsilon_{cu} + f_f} \tag{11b}$$

$$M_{u,Par} = A_f f_f (d - 0.417c). \tag{12}$$

4.4. Rectangular Stress Block Theory

The rectangular stress block parameters, α_1 and β_1 , were determined from the non-linear stress–strain relationship of geopolymers concrete under compression. Two non-linear stress–strain relationships based on the modified Popovics model [42] and calibrated Popovics model [15] were considered to attain these parameters using the concept of an equivalent rectangular stress block. The relationships between α_1 vs. f'_c and β_1 vs. f'_c were further modified by calibrating the analytical results against the experimental data reported in the literature. It was concluded that α_1 is affected

by the curing condition, the mix design of the geopolymer concrete and the compressive strength, whereas β_1 is dependent on the concrete compressive strength only.

Figure 12 illustrates the parabolic and equivalent rectangular stress block of geopolymer concrete under compression. The resultant compressive force of the concrete considering parabolic stress block is represented as $C_c = k_1 k_3 f'_c b c$, where k_1 is the ratio of the average compressive stress to the maximum stress in the compression zone of the structural element, while k_3 is the ratio of the real maximum stress in the compression zone of the structural elements to the concrete strength of the cylinder samples. Tran et al. [36] concluded that k_3 can be considered as 0.9 for heat-cured fly-ash-based geopolymer concrete and as 0.7 for fly-ash and slag-based geopolymer concrete cured under ambient condition.

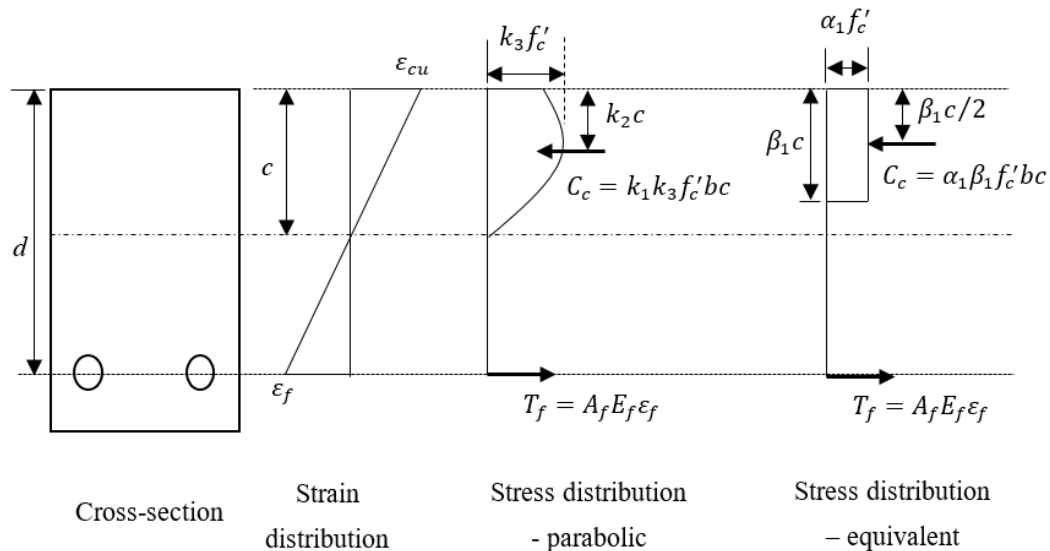


Figure 12. Equivalent rectangular stress block of geopolymer concrete based on [36].

k_2 = ratio of the distance between the extreme compression fibre and the internal compressive force to the depth of the neutral axis.

Using the appropriate k_3 value, rectangular stress block parameter α_1 can be calculated using Equation (13a). Equation (13b) provides the expression to determine the other stress block parameter β_1 . By using these parameters, the location of the neutral axis and the stress acting on the FRP bars can be obtained from Equations (8a) and (8b). The internal moment capacity is calculable from Equation (14).

$$\alpha_1 = \begin{cases} -4.039 \times 10^{-6} (f'_c)^2 - 1.19 \times 10^{-3} f'_c + 0.8542 & \text{when } k_3 = 0.9 \\ -3.142 \times 10^{-6} (f'_c)^2 - 9.25 \times 10^{-4} f'_c + 0.6644 & \text{when } k_3 = 0.7 \end{cases} \quad (13a)$$

$$\beta_1 = 0.8675 - 0.002537 f'_c \quad (13b)$$

$$M_{u,GPC} = A_f f_f \left(d - \frac{\beta_1 c}{2} \right). \quad (14)$$

4.5. Comparison of Theoretical and Experimental Moment Capacity

Since all the FRP-reinforced geopolymer beams were designed for over-reinforcement, the failure strain of the geopolymer concrete is the governing factor. The failure strains of geopolymer concrete vary significantly and were reported to be in the range of 0.0015–0.0050. For comparison, the compression failure strain values obtained in the experiment (Figures 9 and 10) are used to determine the theoretical moment capacity. However, a strain value of 0.003 was also considered as a design value for comparison. All other material and geometrical properties required for the theoretical analysis are taken from Tables 1–3. It should be noted here that no strength reduction factors are used for the

theoretical calculation of ultimate moment capacity. In addition, it is important to point out that the geopolymer mix design used in this study was heat cured, and both fly ash and slag were used. However, Equation (13) accounts for heat-cured fly ash ($k_3 = 0.9$) or ambient-cured fly ash plus slag ($k_3 = 0.7$). Since the samples were heat cured, k_3 is considered to be 0.9 in Equation (13a). Table 8 lists the theoretical moment values obtained using the aforementioned theories as well as experimental moment capacities.

It is evident from the table that the compression failure strain affects the accuracy of the theoretical model. Without the moment reduction factor, all the models are over-estimating the moment capacity. The Canadian Standard is found to be the most accurate with a maximum error of 17%, while the parabolic stress block theory produced the largest errors ranging from 21 to 45%.

If the design failure strain value of 0.003 is used instead of the experimental failure strain, the accuracy generally increases for all models. Again, CSA is found to be the most accurate and safe with a theoretical value less than or equal to the experimental moment capacity. Both the ACI and the rectangular stress block theories (related to geopolymer parameters) are also found to yield satisfactory results with less than 7% error.

Therefore, it can be concluded that even though the ACI and CSA codes are developed for FRP-reinforced OPC concrete, they can certainly be used for FRP-reinforced geopolymer concrete with high accuracy.

Table 8. Comparison of theoretical and experimental ultimate moment capacity.

Beam ID	f_c^f (MPa)	ϵ_{cu}	d (mm)	M_{ext} (kNm)	M_{ACI} (kNm)	M_{CSA} (kNm)	M_{Par} (kNm)	M_{GPC} (kNm)	M_{ACI}/M_{ext}	M_{CSA}/M_{ext}	M_{Par}/M_{ext}	M_{GPC}/M_{ext}
BGF1	60	0.0033	175.3	61.75	63.47	60.80	74.92	62.44	1.03	0.98	1.21	1.01
	61 *	0.0030 ⁺	175.3	61.75	62.08	58.58	73.25	60.91	1.01	0.95	1.19	0.98
BGF2	62	0.0048	175.3	59.79	73.43	69.80	86.83	71.59	1.23	1.17	1.45	1.19
	61 *	0.0030 ⁺	175.3	59.79	62.08	58.58	73.25	60.91	1.04	0.98	1.23	1.02
BCF1	62	0.0040	175.1	55.10	64.47	62.07	76.33	63.27	1.17	1.13	1.39	1.15
	61 *	0.0030 ⁺	175.1	55.10	57.81	55.13	68.15	56.84	1.05	1.00	1.24	1.03
BCF2	60	0.0032	160.1	48.49	50.52	47.93	59.60	49.78	1.04	0.99	1.23	1.03
	61 *	0.0030 ⁺	160.1	48.49	49.91	47.66	58.86	49.04	1.03	0.98	1.21	1.01

* Average compressive strength of geopolymer concrete from Table 1, ⁺ Assumed design value of failure strain.

4.6. Theoretical Comparison between CFRP and GFRP-Reinforced GPC Beam

The reinforcement ratio of GFRP reinforcement used in this study is more than twice the ratio of CFRP. This was intentionally chosen, as it was necessary to validate the design for the industrial project mentioned in Section 1. In order to compare the two FRPs of the same size, a reinforcement ratio of 0.011 was chosen, and the theoretical moment was calculated for geopolymer concrete beams reinforced with #5 GFRP and #5 CFRP. The ultimate moment of the beam with CFRP reinforcement was 32–37% more than that of the beam with GFRP rebar, as shown in Table 9.

Table 9. Comparison of FRP-reinforced geopolymer concrete with the same reinforcement ratio.

Bar	Concrete			Tensile Reinforcement				Moment Capacity		
	Clear Cover (mm)	f'_c (MPa)	ϵ_{cu}	Nominal A_f (mm ²)	Guaranteed f_{fu} (MPa)	E (GPa)	ϵ_{fu} (%)	M_{CSA} (kNm)	M_{ACI} (kNm)	M_{GPC} (kNm)
GFRP #5	50	60	0.003	197.9	1184	62.6	1.89	41.91	43.96	44.57
CFRP #5	50	60	0.003	197.9	1532	140	1.18	57.57	59.90	59.09

5. Conclusions

It should be noted that the conclusions derived from this study are based on testing six beams using fly ash-based heat-cured geopolymer concrete (GPC). The axial rigidity of the CFRP and GFRP bars used were 69 and 84% of the axial rigidity of the conventional steel rebar, resulting in a similar reinforcement ratio for steel and CFRP-reinforced concrete, but the value was 2.5 times higher for GFRP-reinforced GPC.

The present study compared the flexural response of FRP-reinforced geopolymer concrete beams against conventional steel-reinforced concrete. Over-reinforced beams were designed based on both CFRP and GFRP rebars. Accordingly, the failure of RC beams was initiated by steel yielding, whereas the FRP-reinforced beams failed due to concrete crushing. It was concluded that both the FRP and GPC are responsible for the reduction of stiffness by up to 40% while comparing against conventional RC beams. However, the reduction is more for GFRP beams considering the axial rigidity of the bars. While the axial rigidity of GFRP bar was 16% less than the same of steel rebar, stiffness was reduced by 30% in the GFRP-reinforced beam. In contrast, CFRP had 31% less axial rigidity than the steel rebar, but it resulted in a 40% reduction in stiffness.

The flexural strength at the service stage (M_s) is a good indication of the performance of any FRP-reinforced concrete/GPC beam. If the flexural strength at the service stage is defined as 30% of the ultimate moment, a GFRP-reinforced GPC beam yielded 44–48% enhancement in the service moment capacity compared to steel RC beams. This improvement amount was 16–32% for CFRP-reinforced GPC beams despite the fact that the reinforcement ratio of the GFRP beam was 2.5 times higher than the same in CFRP-reinforced beams.

Similar behaviour was observed while comparing the ultimate moment capacity. Both the CFRP and GFRP-reinforced GPC attained a significantly higher ultimate moment capacity than conventional reinforced concrete beams. However, the GFRP-reinforced beam achieved a 17% higher moment capacity than the CFRP-reinforced beam, despite having a 250% higher reinforcement ratio. While comparing the CFRP and GFRP-reinforced geopolymer beams under similar conditions (i.e., same properties of geopolymer concrete and same geometry of the rebar), the CFRP-reinforced GPC beam was found to be 32–37% stronger than the GFRP-reinforced one in terms of ultimate load-carrying capacity.

Four theories/design standards are considered for this comparison—ACI440.1R-15, CAN/CSA S806-12, parabolic stress block theory (for GPC under compression), and equivalent rectangular stress block theory for GPC simplified from the parabolic behaviour of GPC under compression. The failure strain of geopolymer concrete varies significantly within the range of 0.0032–0.0048, and hence, it affects the accuracy of the theoretical prediction. Nevertheless, all theories can predict the capacity satisfactorily, except for the parabolic theory, which was found to be unsafe. ACI and

CSA both had a maximum error margin of 17%, while CSA yielded the most consistently accurate $M_{\text{theoretical}}/M_{\text{experimental}}$. The equivalent rectangular theory also attained values similar to the ACI code.

As suggested in CSA for the design of an FRP-reinforced OPC structure, the beams should be designed as over-reinforced because FRPs are brittle. This study suggests that with the nominal failure strain of 0.003, the CSA and ACI codes can predict the capacity of FRP-reinforced GPC beams fairly well, even though they are based on OPC.

Author Contributions: Conceptualisation, K.G. and M.S.; supervision, K.G. and M.S.; methodology, J.G., K.G. and M.S.; investigation, J.G., K.G. and M.S.; validation, M.S. and J.G.; formal analysis: M.S. and J.G.; Administration, K.G.; writing—original draft preparation, J.G.; writing—review and editing, M.S. and K.G.; funding acquisition, M.S. and K.G. All authors have read and agreed to the published version of the manuscript.

Funding: This research was funded by Geelong Manufacturing Council and Austeng (Australian Engineering Solutions Pty. Ltd.).

Acknowledgments: The authors express their gratitude to other industry partners—Rocla and City of Greater Geelong for their involvement in the project. Furthermore, the authors acknowledge the support and laboratory expertise offered by Lube Velijanoski and Muhammad Ikramul Kabir.

Conflicts of Interest: The authors declare no conflict of interest.

References

1. Wallah, S.; Rangan, B.V. *Low-Calcium Fly Ash-Based Geopolymer Concrete: Long-Term Properties*; Curtin University of Technology: Perth, Australia, 2006.
2. Adak, D.; Mandal, S. Strength and Durability Performance of Fly Ash-Based Process-Modified Geopolymer Concrete. *J. Mater. Civ. Eng.* **2019**, *31*, 04019174. [[CrossRef](#)]
3. Duxson, P.; Fernández-Jiménez, A.; Provis, J.L.; Lukey, G.C.; Palomo, A.; van Deventer, J.S. Geopolymer technology: The current state of the art. *J. Mater. Sci.* **2007**, *42*, 2917–2933. [[CrossRef](#)]
4. Sarker, P. a constitutive model for fly ash-based geopolymer concrete. *Arch. Civ. Eng. Env.* **2008**, *1*, 113–120.
5. Sofi, M.; Van Deventer, J.; Mendis, P.; Lukey, G. Engineering properties of inorganic polymer concretes (IPCs). *Cem. Concr. Res.* **2007**, *37*, 251–257. [[CrossRef](#)]
6. Rubino, F.; Nisticò, A.; Tucci, F.; Carlone, P. Marine Application of Fiber Reinforced Composites: a Review. *J. Mar. Sci. Eng.* **2020**, *8*, 26. [[CrossRef](#)]
7. Balendran, R.; Rana, T.; Maqsood, T.; Tang, W. Application of FRP bars as reinforcement in civil engineering structures. *Struct. Surv.* **2002**, *20*, 62–72. [[CrossRef](#)]
8. Faza, S.S.; Gangarao, H.V. Theoretical and experimental correlation of behavior of concrete beams reinforced with fiber reinforced plastic rebars. *Spec. Publ.* **1993**, *138*, 599–614.
9. Karbhari, V.M.; Seible, F. Fiber-reinforced polymer composites for civil infrastructure in the USA. *Struct. Eng. Int.* **1999**, *9*, 274–277. [[CrossRef](#)]
10. Lloyd, N.; Rangan, B.V. Geopolymer concrete: a review of development and opportunities. In Proceedings of the 35th Conference on Our World in Concrete and Structures, Singapore, 25–27 August 2010; pp. 25–27.
11. Wang, Y.S.; Alrefaei, Y.; Dai, J. Silico-aluminophosphate and alkali-aluminosilicate geopolymers: A comparative review. *Front. Mater.* **2019**, *6*, 106. [[CrossRef](#)]
12. McLellan, B.C.; Williams, R.P.; Lay, J.; Van Riessen, A.; Corder, G.D. Costs and carbon emissions for geopolymer pastes in comparison to ordinary portland cement. *J. Clean. Prod.* **2011**, *19*, 1080–1090. [[CrossRef](#)]
13. Lloyd, N.; Rangan, V. Geopolymer concrete with fly ash. In Proceedings of the Second International Conference on Sustainable Construction Materials and Technologies, Ancona, Italy, 28–30 June 2010; pp. 1493–1504.
14. Khale, D.; Chaudhary, R. Mechanism of geopolymerization and factors influencing its development: A review. *J. Mater. Sci.* **2007**, *42*, 729–746. [[CrossRef](#)]
15. Noushini, A.; Aslani, F.; Castel, A.; Gilbert, R.I.; Uy, B.; Foster, S. Compressive stress-strain model for low-calcium fly ash-based geopolymer and heat-cured Portland cement concrete. *Cem. Concr. Compos.* **2016**, *73*, 36–146. [[CrossRef](#)]
16. Pan, Z.; Sanjayan, J.G.; Rangan, B.V. Fracture properties of geopolymer paste and concrete. *Mag. Concr. Res.* **2011**, *63*, 763–771. [[CrossRef](#)]

17. Sarker, P.K.; Haque, R.; Ramgolam, K.V. Fracture behaviour of heat cured fly ash based geopolymer concrete. *Mater. Des.* **2013**, *44*, 580–586. [[CrossRef](#)]
18. Thomas, R.J.; Peethamparan, S. Alkali-activated concrete: Engineering properties and stress–strain behavior. *Constr. Build. Mater.* **2015**, *93*, 49–56. [[CrossRef](#)]
19. Dattatreya, J.; Rajamane, N.; Sabitha, D.; Ambily, P.; Nataraja, M. Flexural behaviour of reinforced Geopolymer concrete beams. *Int. J. Civ. Struct. Eng.* **2011**, *2*, 138–159.
20. Maranan, G.; Manalo, A.; Benmokrane, B.; Karunasena, W.; Mendis, P. Evaluation of the flexural strength and serviceability of geopolymer concrete beams reinforced with glass-fibre-reinforced polymer (GFRP) bars. *Eng. Struct.* **2015**, *101*, 529–541. [[CrossRef](#)]
21. Nguyen, K.T.; Ahn, N.; Le, T.A.; Lee, K. Theoretical and experimental study on mechanical properties and flexural strength of fly ash-geopolymer concrete. *Constr. Build. Mater.* **2016**, *106*, 65–77. [[CrossRef](#)]
22. Sumajouw, M.; Rangan, B.V. *Low-Calcium Fly Ash-Based Geopolymer Concrete: Reinforced Beams and Columns*; Curtin University of Technology: Perth, Australia, 2006.
23. Yost, J.R.; Radlińska, A.; Ernst, S.; Salera, M.; Martignetti, N.J. Structural behavior of alkali activated fly ash concrete. Part 2: Structural testing and experimental findings. *Mater. Struct.* **2013**, *46*, 449–462. [[CrossRef](#)]
24. Ganesan, N.; Abraham, R.; Raj, S.D.; Sasi, D. Stress–strain behaviour of confined Geopolymer concrete. *Constr. Build. Mater.* **2014**, *73*, 326–331. [[CrossRef](#)]
25. Haider, G.M.; Sanjayan, J.G.; Ranjith, P.G. Complete triaxial stress–strain curves for geopolymer. *Constr. Build. Mater.* **2014**, *69*, 196–202. [[CrossRef](#)]
26. Maranan, G.; Manalo, A.; Karunasena, K.; Benmokrane, B. Bond stress-slip behavior: Case of GFRP bars in geopolymer concrete. *J. Mater. Civ. Eng.* **2015**, *27*, 04014116. [[CrossRef](#)]
27. Okelo, R.; Yuan, R.L. Bond strength of fiber reinforced polymer rebars in normal strength concrete. *J. Compos. Constr.* **2005**, *9*, 203–213. [[CrossRef](#)]
28. Adam, M.A.; Said, M.; Mahmoud, A.A.; Shanour, A.S. Analytical and experimental flexural behavior of concrete beams reinforced with glass fiber reinforced polymers bars. *Constr. Build. Mater.* **2015**, *84*, 354–366. [[CrossRef](#)]
29. Chidananda, S.; Khadiranaikar, R. Flexural Behaviour of Concrete Beams Reinforced With GFRP Rebars. *Int. J. Adv. Res. Ideas Innov. Technol.* **2017**, *3*, 119–128.
30. Goldston, M.; Remennikov, A.; Sheikh, M.N. Experimental investigation of the behaviour of concrete beams reinforced with GFRP bars under static and impact loading. *Eng. Struct.* **2016**, *113*, 220–232. [[CrossRef](#)]
31. Maranan, G.; Manalo, A.; Benmokrane, B.; Karunasena, W.; Mendis, P.; Nguyen, T. Shear behaviour of geopolymer-concrete beams transversely reinforced with continuous rectangular GFRP composite spirals. *Compos. Struct.* **2018**, *187*, 454–465. [[CrossRef](#)]
32. Maranan, G.; Manalo, A.; Benmokrane, B.; Karunasena, W.; Mendis, P.; Nguyen, T. Flexural behavior of geopolymer-concrete beams longitudinally reinforced with GFRP and steel hybrid reinforcements. *Eng. Struct.* **2019**, *182*, 141–152. [[CrossRef](#)]

33. Maranan, G.B.; Manalo, A.C.; Karunasena, W.; Benmokrane, B.; Mendis, P. Flexural response of GFRP-reinforced geopolymer concrete beams. In Proceedings of the 27th Biennial National Conference of the Concrete Institute of Australia (Concrete 2015), Melbourne, Australia, 30 August—2 September 2015; pp. 287–296.
34. Ahmed, H.Q.; Jaf, D.K.; Yaseen, S.A. Flexural strength and failure of geopolymer concrete beams reinforced with carbon fibre-reinforced polymer bars. *Constr. Build. Mater.* **2020**, *231*, 117185. [[CrossRef](#)]
35. Ahmed, H.Q.; Jaf, D.K.; Yaseen, S.A. Comparison of the Flexural Performance and Behaviour of Fly-Ash-Based Geopolymer Concrete Beams Reinforced with CFRP and GFRP Bars. *Adv. Mater. Sci. Eng.* **2020**, *2020*. [[CrossRef](#)]
36. Tran, T.T.; Pham, T.M.; Hao, H. Rectangular Stress-block Parameters for Fly-ash and Slag Based Geopolymer Concrete. *Structures* **2019**, *19*, 143–155. [[CrossRef](#)]
37. Ahmed, H.Q.; Jaf, D.K.; Yaseen, S.A. Flexural Capacity and Behaviour of Geopolymer Concrete Beams Reinforced with Glass Fibre-Reinforced Polymer Bars. *Int. J. Concr. Struct. Mater.* **2020**, *14*, 1–16. [[CrossRef](#)]
38. ACI. *Guide for the Design and Construction of Structural Concrete Reinforced with Fiber Reinforced Polymer (FRP) Bars (ACI 440.1R-15)*; American Concrete Institute: Farmington Hills, MI, USA, 2015.
39. CSA. *Design and Construction of Building Structure with Fibre-Reinforced Polymer (CAN/CSA S806-12)*; Canadian Standards Association: Toronto, AB, Canada, 2012.
40. Newhook, J.; Svecova, D. Reinforcing Concrete Structures with Fibre Reinforced Polymers: Design manual no. 3. *Can. ISIS Can. Corp.* **2007**, *151*, 449–458.
41. Bischoff, P.; Gross, S.; Ospina, C. The story behind proposed changes to ACI 440 deflection requirements for FRP-reinforced concrete. *Spec. Publ.* **2009**, *264*, 53–76.
42. Sarker, P.K. Analysis of geopolymer concrete columns. *Mater. Struct.* **2009**, *42*, 715–724. [[CrossRef](#)]

Publisher's Note: MDPI stays neutral with regard to jurisdictional claims in published maps and institutional affiliations.



© 2020 by the authors. Licensee MDPI, Basel, Switzerland. This article is an open access article distributed under the terms and conditions of the Creative Commons Attribution (CC BY) license (<http://creativecommons.org/licenses/by/4.0/>).